

Restoration of AFM Images that were Produced using the Estimated AFM Tip at Three Different Scanning Speeds

AHMED AHTAIBA

Electrical and Electronic Engineering Department,
Sirte University,
Sirte,
LIBYA

Abstract: - The contact between the sample and the AFM tip causes distortions in all atomic force microscope (AFM) pictures. With the three-dimensional tip form in hand, the distorted picture may be straightened out and the surface structure's original state "restored" using deconvolution methods. Compared to the initial distorted image, the restored image provides a more realistic portrayal of the sample's true 3D surface. In order to estimate the impulse response of the AFM, this work presents a new method that uses contact mode AFM to measure the dimensions of a micro-cylinder. Subsequent AFM pictures are subsequently restored using the predicted impulse response.

Key-Words: - AFM, image restoration, scanning speed, pillar sample, AFM tip.

Received: March 24, 2024. Revised: October 9, 2024. Accepted: November 13, 2024. Published: December 23, 2024.

1 Introduction

Atomic force microscopes (AFMs) are highly specialized tools capable of analyzing the surfaces of metals, semiconductors, and insulators. They operate effectively in various environments, including vacuum, liquid, or air, and are extremely sensitive to atomic forces. These microscopes provide ultra-high resolution, allowing them to image, measure, manipulate, and probe objects at the micro and nanoscale. AFMs have a significant advantage over other high-resolution microscopes like the Scanning Tunneling Microscope (STM) in that they can examine both conducting and non-conducting materials.

Deformities in AFM images are caused by the sample's interaction with the impulse response of the AFM, despite their capabilities. By obtaining the impulse response, one may rectify the distortions and restore the original surface structure, usually by employing deconvolution techniques. This process results in a more accurate representation of the sample's actual two-dimensional surface compared to the initial, deformed picture. The difficulty of accurately re-creating surface topography from AFM samples has been the subject of several research efforts. Notably, researchers such as Pingali and Jain employed mathematical morphological operators to successfully restore AFM images.

[1], after Keller and Franke used photos of known samples to rebuild the AFM tip shape, they

used that shape to recover AFM images, [2]. Villarrubia developed a method for blind tip reconstruction, which is also grounded in mathematical morphology, [3]. Dongmo applied this algorithm to reconstruct the tip of a stylus profilometer, afterwards, we'll compare the SEM picture with the rebuilt tip form [4]. Subsequently, Todd showed that AFM picture noise skews the tip shape estimate, and he suggested a better way to improve the method, [5]. The practical application of the algorithm also considered factors like sampling intervals and instrumental noise, [6]. Following this, they laid up some ground rules and set up several suitable experiments to test the blind estimation process. In this work, a technique is offered for approximating 3 dimensions AFM tip shape from the measurement of a micro-cylinder with well-known and independently measured dimensions. If the same tip is used under identical measurement condition, the predicted tip shape can be utilized to reconstruct AFM pictures taken at a later time. The ability to deduce the impulses responses of the AFM is a notable feature of this approach. The efficacy of this novel method in repairing AFM pictures has been confirmed by means of both virtual and physical experimental AFM pictures.

2 The Impulse Response of an AFM is Estimated by Utilizing a Cylindrical Pillar Sample

The HS-100MG standard sample, with its defined dimensions, silicon construction, and 2D array of tiny cylindrical columns, was measured using the contact mode AFM. After taking this AFM measurement, we chose one pillar out of the picture. As seen in Figure 1(a), setting a threshold allowed us to calculate the size of the top of the column in the AFM picture, which is nearly a complete circle. In Figure 1(b), we can see the outcome of applying the Canny edge detection technique to determine the pillar's outside border. Figure 1(c) depicts the steps used to estimate the data on tip distortion around the column's perimeter by increasing the circle's outside edge. In this case, d represents the cylinder's diameter, the size expansion was between around $1.2d$ and $2d$. The data for the cylinder's tips, which had been originally placed around its outside edge, were then transferred radially inwards to the center of the cylinder that had been removed using Breshnam's line method. In Figure 1(d), we can see the result of using the suggested method, which is the predicted form of the 3-dimensional AFM impulse response.

A priori knowledge of non- negativity and flux conservation is incorporated into the widely-used Lucy-Richardson algorithm. Through an iterative approach, it is able to recover AFM pictures. The fundamental premise is that there is a connection between the ideal image of the AFM and its impulse response. Lucy-Richardson optimizes the picture's likelihood function using Poisson statistics as a model, [7], [8]. Typically, the hazy image is used as the initial estimate. Some examples of iterative algorithms include the Lucy-Richardson method, [9], [10], [11].

$$f_{k+1}(x, y) = f_k(x, y) \frac{g(x, y) * h(-x, -y)}{[h(x, y) * f_k(x, y)] * h(-x, -y)} \quad (1)$$

Where g, x, y represents the blurred AFM picture, $(-x, -y)$ denotes the transpose of the system's impulse response, and $f_k(x, y)$ represents the prior estimate of the AFM image, $h(x, y)$ denotes the impulse response of the AFM system, and $f_{k+1}(x, y)$ signifies the current estimate of the AFM picture.

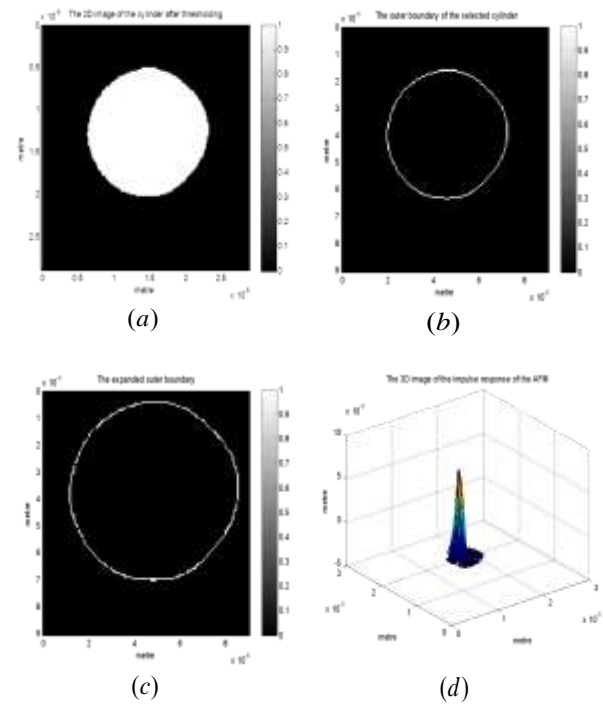


Fig. 1: Standard operating procedure (SOP) for determining the AFM's impulse response: (a) first, a standard sample with a cylinder of predetermined dimensions is subjected to a threshold. Then, the cylinder's position in the image is determined by drawing its outer boundary. To remove the cylinder's pixels from the image, the outer boundary is enlarged. Finally, the AFM's impulse response is extracted.

3 Experimental Results

3.1 AFM Image Restoration at a Scanning Rate of 1 Hz

Two genuine samples were analyzed at a scanning speed of 1 H-z using contact mode atomic force microscopy (AFM). One of the samples was a grid of elevated square pillars, and the other was a true specimen with an array of raised cylindrical pillars. The identical methods described before and illustrated in Figure 1 were utilized while scanning at this pace. After the AFM impulse response was estimated at this speed, the raw AFM image, which had been captured at the same detecting speed as the AFM impulse response, and the derived impulse response were subjected to a Lucy-Richardson deconvolution procedure. As shown in Figure 2(c), the recovered AFM picture showed qualitative improvements in terms of fidelity after using the Lucy-Richardson deconvolution approach to an

AFM image of a genuine material with cylindrical pillars.

The numerical findings for the original AFM picture (Figure 2(a)) and the recovered image (Figure 2(c)) at a detecting speed of 1 Hz are provided in Table 1. We compared the AFM image's first row of pillar measurements to the repaired AFM image's corresponding row. In the AFM picture, the height (H1) of the first pillar (P1,1) is 91.38 nm, while in the restored image, the equivalent height (H2) is 91.68 nm. This pillar is situated near the row center, at (X = 2.647 μm , Y = 2.441 μm). There is a 0.3 nm height disparity between H1 and H2, which is equal to a 0.327% difference (D%). H1 measures 88.59 nm for the second pillar (P1,2) in the same row of the AFM picture, which is located at (X = 7.617 μm , Y = 2.441 μm). In the corrected picture, the matching height (H2) is 88.89 nanometers. With a height disparity of 0.3 nm, or 0.337%, between H1 and H2 is the result. According to the AFM picture, the third pillar (P1,3) stands at 86.24 nm in height (H1), with coordinates (X = 12.62 μm , Y = 2.441 μm). In the reconstructed picture, the comparable height (H2) is 86.52 nm, which is different from the original by 0.28 nm, or 0.323%.

When we compare the height disparities between H-1 and H-2 at a scanning speed of 1 Hz, we find that the percentage differences are minor, with the lowest being 0.323%. The 1st row of pillars in the AFM picture (Figure 2(a)) and their corresponding row in the reconstructed image (Figure 2(c)) are compared quantitatively in Table 1.

Reconstructing future AFM pictures is possible with the help of the Lucy-Richardson deconvolution process, which uses the raw AFM picture and the AFM's impulse response (already stated and shown in Figure 1).

Table 1. A comparison of quantitative values of the first row of pillars in the AFM image (Figure 2(a)) with the values of the corresponding row in the restored image (Figure 2(c))

Pillar position	P(1,1)	P(1,2)	P(1,3)
X[μm]	2.647	7.617	12.62
Y[μm]	2.441	2.441	2.441
H1[nm]	91.38	88.59	86.24
H2[nm]	91.68	88.89	86.52
D[nm]	0.3	0.3	0.28
D%	0.327%	0.337%	0.323%

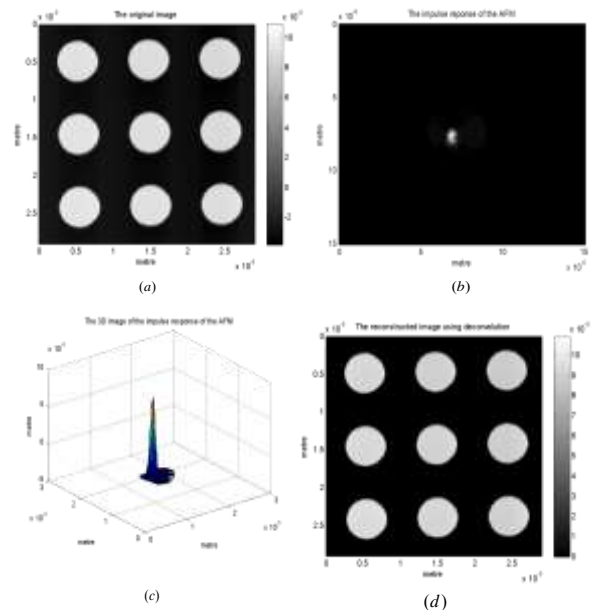


Fig. 2: A juxtaposition of the original experimental picture of the AFM and the recovered picture of the AFM acquired using the suggested method with a scanning speed of 1 Hz: (a) a picture of the real sample made with an AFM tip, showing cylindrical pillars; (b) a two-dimensional depiction of the AFM's impulse response; (c) a three-dimensional illustration of the AFM's impulse response; and (d) an image of the restored The AFM picture and the estimated impulse response were used in a Lucy-Richardson deconvolution procedure to get the AFM representation

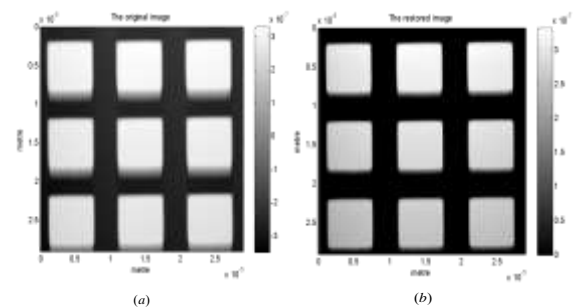


Fig. 3: With a scanning speed of 1 Hz, the experimental raw AFM picture and the recovered AFM image, which was created using the suggested approach. (a) A picture of the actual sample with square pillars as captured by an AFM tip; (b) A picture of the cleaned-up AFM output made from the AFM picture plus the estimated impulse response of the AFM using Lucy-Richardson deconvolution.

Figure 3(a) and Figure 3(b) illustrate a comparison for the original AFM topography image acquired at a 1 Hz scanning speed and the recovered

AFM image produced by the Lucy-Richardson deconvolution method, respectively. The unprocessed picture illustrates a series of raised square columns. Figure 3(b) demonstrates that the Lucy-Richardson deconvolution approach is successful, resulting in a more accurate restored image.

3.2 Bringing Back AFM Pictures while Scanning at 2 Hz

All previously measured samples at 1 Hz are employed here. Subsequently, the experimental images of these specific materials made use of an AFM scanning rate of 2 Hz. Images of an experimental sample with a grid of raised square pillars (Figure 4(a)) and a configuration of raised cylindrical pillars (Figure 5(a)) are presented, respectively. Using a Lucy-Richardson deconvolution process on the raw AFM picture and the estimated AFM impulse response, as described in Section 2 and shown in Figure 4(c), the experimental images captured by the AFM at a 2 Hz scanning speed may be recovered. Consequently, in comparison to the unprocessed experimental AFM images in Figure 4(d) and Figure 5(b), the restored images exhibit a marked enhancement in fidelity. Table 2 compares the matching quantitative values in the AFM picture (Figure 4(a)) and the restored image (Figure 4(d)) for the first row of pillars. Using a scanning speed of 2 Hz, the AFM image was measured. Pillar P(1,1), situated at coordinates ($X = 2.647 \mu\text{m}$, $Y = 2.441 \mu\text{m}$), has a height (H1) of 91.59 nm. In the corrected picture, the matching height (H2) is 92.14 nm. The dissimilarity (D) between the two hydrogen bonds, H1 and H2, is 0.55 nm, or 0.596%.

The first pillar, P(1,2), stands at a height of 94.2 nm, with coordinates ($X = 7.617 \mu\text{m}$, $Y = 2.441 \mu\text{m}$). In the corrected picture, the matching height (H2) is 94.76 nm. A 0.56 nm discrepancy, or 0.590% percentage difference, separates H1 and H2 for P(1,2).

The first pillar, P(1,3), stands at 86.65 nm in height, with coordinates ($X = 12.62 \mu\text{m}$, $Y = 2.441 \mu\text{m}$). In the corrected picture, the matching height (H2) is 87.17 nm. For P(1,3), there is a 0.52 nm discrepancy between H1 and H2, which translates to a 0.596% percentage difference.

At 0.590 percent, P(1,2) has the narrowest percentage discrepancy between H1 and H2 in Table 2.

Table 2 shows the numbers for the first row of pillars in both the AFM picture (Figure 4(a)) and the reconstructed image (Figure 4(c)).

Table 2. A comparison of quantitative values of the first row of pillars in the AFM image (Figure 4(a)) with the values of the corresponding row in the restored image (Figure 4(c))

Pillar position	P(1,1)	P(1,2)	P(1,3)
X[μm]	2.647	7.617	12.62
Y[μm]	2.441	2.441	2.441
H1[nm]	91.59	94.2	86.65
H2[nm]	92.14	94.76	87.17
D[nm]	0.55	0.56	0.52
D%	0.596%	0.590%	0.596%

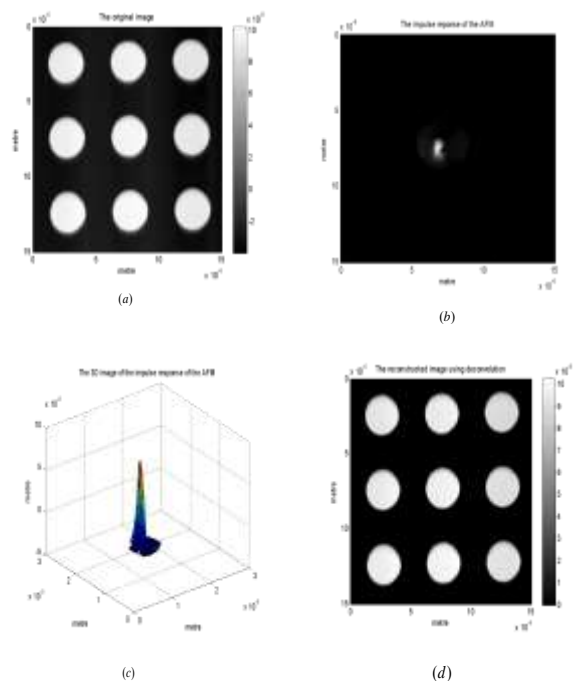


Fig. 4: Result of applying the suggested method at a scanning speed of 2 Hz to an AFM picture, compared to the original experimental AFM image: (a) a picture of the real sample with cylindrical pillars taken by the tip of the AFM; (b) a two-dimensional depiction of the impulse response of the AFM; (c) the three-dimensional depiction of the AFM's impulse response; and (d) the reconstructed image of the AFM subsequent to the application of an AFM picture and its predicted impulse response by a Lucy-Richardson deconvolution method.

Figure 5 shows the raw AFM picture and the restored AFM picture, both generated using the suggested approach at a scanning speed of 2 Hz.

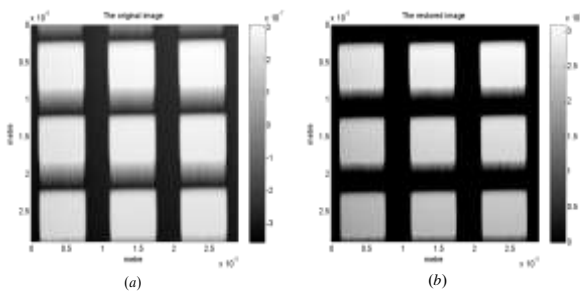


Fig. 5: The raw AFM picture and the restored AFM picture both generated using the suggested approach at a scanning speed of 2 H-z. (a) the original AFM picture of the sample with square pillars measured by the tip; (b) the recovered AFM image created by merging the original image with the estimated impulse response from the AFM using the Lucy-Richardson deconvolution method.

3.3 AFM Image Restoration at a Scanning Rate of 2.5 Hz

The experimental pictures of an actual sample with a grid of raised square pillars and an array of raised cylindrical pillars are shown in Figure 6(a) and Figure 7(a), respectively. Nevertheless, these pictures have been assessed using the AFM at a 2.5 Hz scanning rate in the subsequent set of data. Using a Lucy-Richardson deconvolution technique, which was described in Section 2, on the original AFM picture and the impulse response obtained as shown in Figure 6(c), the AFM images of the two actual samples may be restored. Figures 6(d) and 7(b) display the recovered AFM pictures that were created by implementing the deconvolution procedure, correspondingly. By eliminating the impacts of the AFM impulse response convolution that was present in the initial hazy raw AFM photos, the deconvolution technique significantly enhanced the quality of the recovered AFM images. Table 3 compares numerical data from the first row of pillars in the AFM picture (Figure 6(a)) with numerical data from the corresponding row in the restored image (Figure 6(d)). The scanning speed used to measure this AFM picture was 2.5 Hz. At coordinates ($X = 2.647 \mu\text{m}$, $Y = 2.441 \mu\text{m}$), the pillar P(1,1) stands at a height of 93.45 nm, also known as H1. In the corrected picture, the matching height (H2) is 94.3 nm. For P(1,1), there is a 0.901% discrepancy between H1 and H2, which is 0.85 nm.

In the restored picture, the equivalent height (H2) is 92.57 nm, while for the second pillar in the first row, P(1,2), at a location ($X = 7.617 \mu\text{m}$, $Y = 2.441 \mu\text{m}$), the height (H1) is 91.73 nm. In terms of

percentage, the 0.84 nm gap between H1 and H2 is equivalent to 0.907%.

In the first row, the third pillar (P(1,3)) has a height (H1) of 88.67 nm. H2 stands for 89.49 nanometers in the corrected picture. With a percentage difference of 0.916% and a difference of 0.82 nm, H1 and H2 are not identical. With respect to P(1,1), the table shows that the minimal percentage difference between H1 and H2 is 0.901%.

The first row of pillars in the AFM picture (Figure 6(a)) and the corresponding row in the restored image (Figure 6(d)) were compared quantitatively in Table 3.

Table 3. A comparison of quantitative values of the first row of pillars in the AFM image (Figure 6(a)) with the values of the corresponding row in the restored image (Figure 6(d))

Pillar position	P(1,1)	P(1,2)	P(1,3)
X[μm]	2.647	7.617	12.62
Y[μm]	2.441	2.441	2.441
H1[nm]	93.45	91.73	88.67
H2[nm]	94.3	92.57	89.49
D[nm]	0.85	0.84	0.82
D%	0.901%	0.907%	0.916%

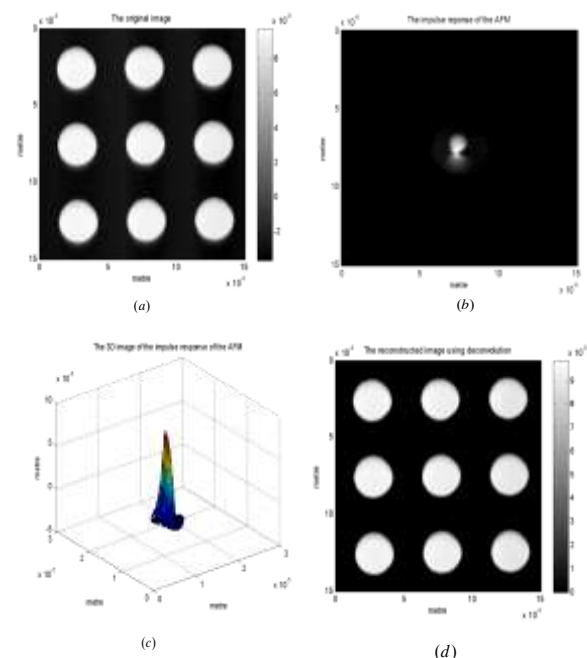


Fig. 6: The unprocessed experimental AFM image is contrasted with the recovered AFM image, which was generated using the recommended procedure using a 2.5 H-z scanning rate. (a) One view shows the sample with cylindrical pillars as measured by an AFM tip; (b) another shows the AFM impulse

response in two dimensions; (c) a third shows the AFM impulse response in three dimensions; and (d) the last view is the recovered AFM image, which is made by applying a Lucy-Richardson deconvolution technique to both the AFM image and the expected impulse response of the AFM.

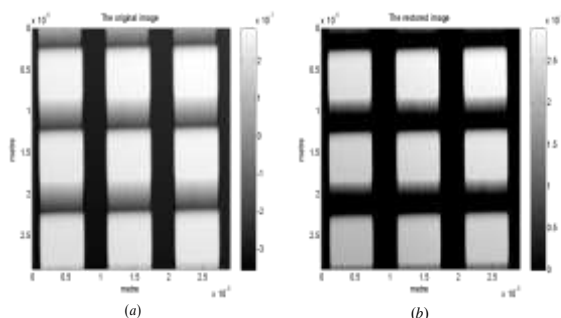


Fig. 7: The original experimental AFM picture and the recovered AFM image, which were generated using the recommended method at a scanning speed of 2.5 H-z. (a) an AFM-captured picture of the actual sample with square pillars; (b) a recovered AFM picture created by merging the original and predicted AFM impulse responses using the Lucy-Richardson deconvolution technique.

4 Conclusion

In order to restore AFM pictures and approximate the AFM tip, this research presents a new method.

The study's experimental findings are shown by a number of instances. The two authentic examples that were scrutinized were a grid of raised square pillars and an array of elevated cylindrical pillars. The actual samples were measured using three distinct scanning rates: 1 Hz, 2 H-z, and 2.5 H-z. The unprocessed AFM pictures and the impulse response determined for each scanning speed were combined using a Lucy-Richardson deconvolution technique after the AFM impulse response was estimated. The measured AFM height pictures were rendered more faithfully after undergoing this deconvolution procedure.

You can see the comparison between the AFM picture and the reconstructed image at 1 H-z, 2 H-z, and 2.5 H-z scanning rates for the first row of pillars quantitative indicators in Table 1, Table 2 and Table 3, respectively.

References:

- [1] A. Ahtaiba, The Improvement in The AFM Image after Applying a Lucy-Richardson Deconvolution Algorithm using a New Technique for Estimating the AFM Tip Shape from the Square Sample, *WSEAS Transactions on Signal Processing*, Vol. 19, 2023, pp.103-107, <https://doi.org/10.37394/232014.2023.19.11>.
- [2] R. Gonzalez, *Digital Image Processing Using Matlab*, Second Edition, GateMark Publishing, 2008.
- [3] G. S. Pingali and R.Jain, *Restoration of Scanning Probe Microscope Images*, In Application Of Computer Vision, Palm Springs, CA, USA, 1992.
- [4] D. J. Keller and F. S.Franke, "Envelope Reconstruction of Probe Microscope Images," *Surface Science*, P. 11, 1993.
- [5] J.S.Villarrubia, Algorithms for Scanned Probe Microscope Image Simulation Surface Reconstruction and Tip Estimation, *Journal of Research of The National Institute of Standards and Technology*, Vol.04, 1997, PP. 425-454.
- [6] L.S.Dongmo, J.S. Villarrubia, S.N.Jones, T.B.Renegar, M.T.Postek, and J.F.Song, Experimental Test of Blind Tip Reconstruction for Scanning Probe Microscopy, *Ultramicroscopy*, Vol. 85, 2000, PP. 141 - 153.
- [7] T. Brain and E. Steven, A Method to Improve the Quantitative Analysis of SFM Images at the Nanoscale, *Surf. Sci.*, 2001.
- [8] D.Tranchida, S.Piccarolo, and R.A.C.Deblieck, Some Experimental Issues of AFM Tip Blind Estimation: The Effect of Noise and Resolution, *Meas. Sci. Technol.*, Vol.17,2006 PP. 2630-2636.
- [9] L. Lucy, An Iterative Technique for the Rectification of Observed Distributions, *The Astronomical Journal*, Vol. 79, No.6, 1974, pp. 745-754.
- [10] W. Richardson, Bayesian-Based Iterative Method of Image Restoration, *J. Opt. Soc. Am.*, Vol. 62, No. 1, 1972, pp. 55-59.
- [11] R. Gonzalez, *Digital Image Processing Using Matlab*, Second Edition, GateMark Publishing, 2009.

Contribution of Individual Authors to the Creation of a Scientific Article (Ghostwriting Policy)

The authors equally contributed in the present research, at all stages from the formulation of the problem to the final findings and solution.

Sources of Funding for Research Presented in a Scientific Article or Scientific Article Itself

No funding was received for conducting this study.

Conflict of Interest

The authors have no conflicts of interest to declare.

Creative Commons Attribution License 4.0 (Attribution 4.0 International, CC BY 4.0)

This article is published under the terms of the Creative Commons Attribution License 4.0

https://creativecommons.org/licenses/by/4.0/deed.en_US